
How Do Diffusion Models Improve Adversarial Robustness?

Liu Yuezhang
 UT Austin
 lyz@utexas.edu

Xue-Xin Wei
 UT Austin
 weixx@utexas.edu

Abstract

Recent findings suggest that diffusion models significantly enhance empirical adversarial robustness. While some intuitive explanations have been proposed, the precise mechanisms underlying these improvements remain unclear. In this work, we systematically investigate how and how well diffusion models improve adversarial robustness. First, we observe that diffusion models intriguingly increase, rather than decrease, the ℓ_p distance to clean samples—challenging the intuition that purification denoises inputs closer to the original data. Second, we find that the purified images are heavily influenced by the internal randomness of diffusion models, where a compression effect arises within each randomness configuration. Motivated by this observation, we evaluate robustness under fixed randomness and find that the improvement drops to approximately 24% on CIFAR-10—substantially lower than prior reports approaching 70%. Importantly, we show that this remaining robustness gain strongly correlates with the model’s ability to compress the input space, revealing the compression rate as a reliable robustness indicator without requiring gradient-based analysis. Our findings provide novel insights into the mechanisms underlying diffusion-based purification, and offer guidance for developing more effective and principled adversarial purification systems.

1 Introduction

Neural networks are vulnerable to small adversarial perturbations (Szegedy et al., 2013; Goodfellow et al., 2014). The lack of robustness presents a fundamental problem of artificial learning systems. Adversarial training (Madry et al., 2017) has been proposed as an effective method to overcome this problem under certain scenarios (Shafahi et al., 2019; Pang et al., 2020; Wang et al., 2021). However, research has found that training with a specific attack usually sacrifices the robustness against other types of perturbations (Schott et al., 2018; Ford et al., 2019; Yin et al., 2019), indicating that adversarial training overfits the attack rather than achieving an overall robustness improvement.

Adversarial purification represents an alternative promising path toward adversarial robustness. This approach typically uses generative models to purify the stimulus before passing to a classifier (Song et al., 2018; Samangouei et al., 2018; Shi et al., 2021; Yoon et al., 2021). The basic idea is to leverage the image priors learned in generative models to project adversarial perturbations back toward the image manifold. Intuitively, the performance of such purification should depend on how well the generative models encode the probability distribution over natural images. Recently, adversarial purification based on diffusion models (Ho et al., 2020; Song et al., 2020b) (DiffPure) was reported to show impressive improvements against various empirical attacks on multiple datasets (Nie et al., 2022). The idea of using diffusion models as denoisers was further combined with the deonise smoothing framework (Cohen et al., 2019; Salman et al., 2020) to improve certificated robustness (Carlini et al., 2022; Xiao et al., 2023). However, more recent work (Lee & Kim, 2023; Li et al., 2025) show that there was an overestimate of the robustness improvement from the DiffPure method. Overall, despite

some promising empirical results, the underlying mechanisms of empirical robustness improvement from diffusion models (how), as well as a proper robustness evaluation with randomness (how well), were still not well understood.

To close this important gap, we systematically investigated how and how well diffusion models improve adversarial robustness. In this paper, we report a set of surprising phenomena of diffusion models, and identify the key mechanisms for robustness improvements under diffusion-model-based adversarial purification. Our main contributions are summarized below:

- **Revealing intriguing behaviors of diffusion-based purification.** We observe that, somewhat surprisingly, diffusion models increase—rather than decrease— ℓ_p distances to clean samples (Sec. 3.1), with the purified states being heavily influenced by randomness (Sec. 3.2).
- **Measuring robustness gains without stochasticity.** After controlling for randomness, the net adversarial robustness gain drops to 23.7% on CIFAR-10—substantially lower than the $\sim 70\%$ (or 46% with EOT) reported with full stochasticity (Sec. 4).
- **Discovering that the compression rate of the image space predicts robustness.** This net robustness gain is well explained by a compression-based theory, with the compression rate being a strong indicator of robustness that does not require gradient calculations (Sec. 5).

Overall, the empirically observed robustness improvements from diffusion models stem from two sources: stochasticity, and a deterministic compression effect of image space.

2 Related work and preliminaries

Generative models for adversarial purification Unlike adversarial training which directly augments the classifier training with adversarial attacks, adversarial purification intends to first “purify” the perturbed image before classification. Generative models are usually utilized as the purification system, such as denoising autoencoder (Gu & Rigazio, 2014), denoising U-Net (Liao et al., 2018), PixelCNN (Song et al., 2018) and GAN (Samangouei et al., 2018).

Diffusion models (Ho et al., 2020; Song et al., 2020b) set the SOTA performances on image generation, and represent a natural choice for adversarial purification. Nie et al. (2022) proposed the DiffPure framework, which utilized both the forward and reverse process and achieved promising empirical robustness comparable with adversarial training on multiple benchmarks. Similar improvements were reported with guided diffusion models (Wang et al., 2022). These studies led to substantial interest in applying diffusion models for adversarial purification in various domains, including auditory data (Wu et al., 2022) and 3D point clouds (Sun et al., 2023). Recently, other techniques, such as adversarial guidance (Lin et al., 2024) and bridge models (ADBM) (Li et al., 2025), were introduced to further enhance robustness. Another line of research applies diffusion models to improve certificated robustness Cohen et al. (2019). Carlini et al. (2022) found that plugging diffusion models as a denoiser into the denoised smoothing framework (Salman et al., 2020) can lead to non-trivial certificated robustness. Xiao et al. (2023) further developed this method and studied the improvement in certificated robustness.

Diffusion models and randomness Diffusion models consist of forward diffusion and reverse denoising processes. The forward process of Denoising Diffusion Probabilistic Models (DDPM) (Ho et al., 2020) is

$$\mathbf{x}_t = \sqrt{\alpha_t} \mathbf{x}_{t-1} + \sqrt{1 - \alpha_t} \boldsymbol{\epsilon}, \quad \boldsymbol{\epsilon} \sim \mathcal{N}(\mathbf{0}, \mathbf{I}), \quad (1)$$

in which the $\boldsymbol{\epsilon}$ will introduce randomness. Further, the reverse process

$$\mathbf{x}_{t-1} = \frac{1}{\sqrt{\alpha_t}} \left(\mathbf{x}_t - \frac{1 - \alpha_t}{\sqrt{1 - \bar{\alpha}_t}} \boldsymbol{\epsilon}_\theta(\mathbf{x}_t, t) \right) + \sigma_t \mathbf{z}, \quad \mathbf{z} \sim \mathcal{N}(\mathbf{0}, \mathbf{I}) \quad (2)$$

also introduces randomness through \mathbf{z} . Notably, deterministic reverse process has been proposed, e.g., in Denoising Diffusion Implicit Models (DDIM) (Song et al., 2020a) the reverse process

$$\mathbf{x}_{t-1} = \sqrt{\bar{\alpha}_{t-1}} \hat{\mathbf{x}}_0 + \sqrt{1 - \bar{\alpha}_{t-1}} \boldsymbol{\epsilon}_\theta(\mathbf{x}_t, t), \quad \hat{\mathbf{x}}_0 = \frac{\mathbf{x}_t - \sqrt{1 - \bar{\alpha}_t} \boldsymbol{\epsilon}_\theta(\mathbf{x}_t, t)}{\sqrt{\bar{\alpha}_t}} \quad (3)$$

is fully deterministic and thus does not involve randomness.

Empirical evaluation of the robustness of diffusion models Such randomness may raise concerns about gradient masking in robustness evaluation (Papernot et al., 2017), which provides a false sense of robustness against gradient-based attacks (Tramèr et al., 2018). Athalye et al. (2018) further identified that randomness could cause gradient masking as “stochastic gradients”, and proposed the expectation-over-transformation (EOT) which became the standard evaluation for stochastic gradients (Carlini et al., 2019). Additionally, under the assumption that purification systems bring adversarial examples close to clean data, Backward Pass Differentiable Approximation (BPDA) (Athalye et al., 2018) was introduced as a method for evaluating purification-based defenses. However, the proper treatment of randomness in robustness evaluation remains a subject of debate (Gao et al., 2022; Yoon et al., 2021).

In diffusion models, internal randomness and the substantial computational overhead of full-gradient computation make robustness evaluation particularly difficult. The original DiffPure paper applied AutoAttack (Croce & Hein, 2020) with augmented SDE-based gradient estimation and reported a robust accuracy of 70.64% on CIFAR-10. However, through a comprehensive experimental evaluation, (Lee & Kim, 2023) found that the robustness improvements from diffusion models were over-estimated. They recommended using the PGD-EOT with full gradients directly, and estimated the robustness around 46.84%. Recently, Li et al. (2025) also challenged the original evaluation and reported a comparable robustness estimate of 45.83%.

3 Intriguing behaviors of diffusion models under adversarial purification

Overview and notations We first introduce key notations for the rest of the paper, and then provide an overview of our framework (see Fig. 1b). Denote \mathbf{x}_0 as a clean image, and \mathbf{x} as its perturbed version, so that

$$\mathbf{x} = \mathbf{x}_0 + \epsilon \boldsymbol{\eta}, \quad (4)$$

where $\boldsymbol{\eta}$ is the normalized adversarial perturbation, and ϵ controls the magnitude of the attack. Further denote f as the purification system and g as the readout classifier. Adversarial purification typically consists of two steps: (i) purifying the perturbed image using f ; (ii) classifying the output using g :

$$\hat{\mathbf{x}} = f(\mathbf{x}), \quad \mathbf{y} = g(\hat{\mathbf{x}}). \quad (5)$$

Importantly, the purification system may be stochastic. In particular, this is true for diffusion-model-based purification. Denote ξ as a randomness configuration, which, practically, is determined by a series of random seeds governing the stochastic process in diffusion models. Denote f_ξ as the mapping induced by ξ . Suppose M is the small image neighborhood defined the budget of the adversarial attack, we denote \tilde{M}_ξ as the transformed image neighborhood induced by ξ . Note that when changing ξ , \tilde{M}_ξ would also change.

Since adversarial attacks often operate at a small perturbation scale ϵ , for each ξ , we consider the first-order Taylor expansion of $f_\xi(\mathbf{x})$ around \mathbf{x}_0 :

$$f_\xi(\mathbf{x}) = f_\xi(\mathbf{x}_0 + \epsilon \boldsymbol{\eta}) = \underbrace{f_\xi(\mathbf{x}_0)}_{\text{anchor point}} + \epsilon \underbrace{J_{f_\xi}(\mathbf{x}_0)}_{\text{compression}} \boldsymbol{\eta} + o(\epsilon), \quad (6)$$

where $f_\xi(\mathbf{x}_0)$ represents the purified clean image, which we will refer to as the “*anchor point*”. The Jacobian matrix $J_{f_\xi}(\mathbf{x}_0)$ quantifies the local linear transformation induced by f_ξ .

3.1 Diffusion models push perturbed images further away from clean images

While the exact mechanisms underlying the robustness improvements from diffusion models remain unclear, prior work has suggested intuitive explanations, *e.g.*, diffusion models may recover clean samples through reverse denoising (Nie et al., 2022). This motivates us to first test a “denoising” hypothesis, that is, diffusion models reduce the ℓ_p distance to clean images during adversarial purification. Intuitively, if a purification system consistently reduces ℓ_p distances of a perturbed image to the clean image, it would effectively transform an adversarial perturbation into one of smaller magnitude, thereby enhancing robustness (see Fig.1a).

Diffusion models increase ℓ_p distances to clean images after purification. To test whether diffusion models reduce the distance between adversarial and clean images, we conducted a series of experiments. From a clean image, we generated an adversarial example, then applied adversarial purification via diffusion models, and finally measured the distance between the purified image and

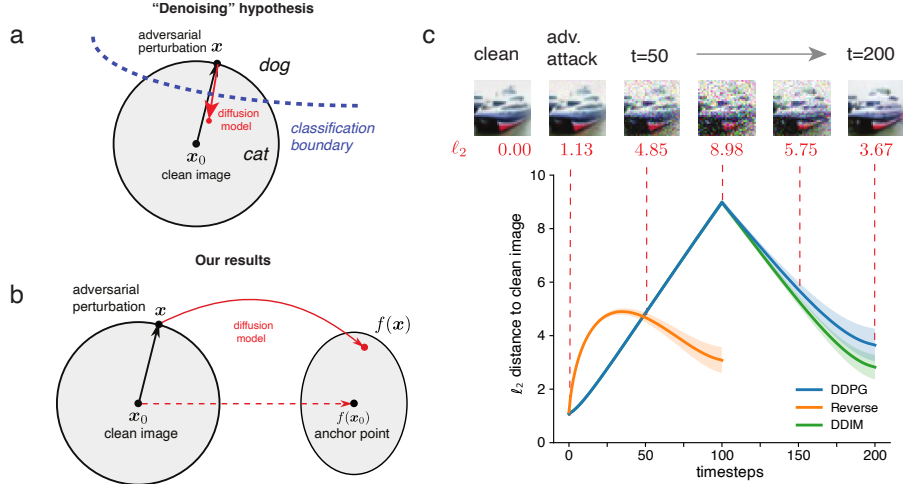


Figure 1: **Diffusion models purify states away from the clean images.** (a) Schematic showing a common hypothesis that diffusion models improve robustness by ‘denoising’ inputs toward the clean image. (b) Summary of our findings, which challenge the denoising hypothesis. (c) Measured ℓ_2 distances to clean images on CIFAR-10 during purification. We track the distances between intermediate purified states and clean images, using PGD attacks ($\ell_\infty = 8/255$) as initialization. Across all methods, the purified outputs are consistently farther away from the clean image.

the original clean image. Surprisingly, we found that the ℓ_2 distance to the clean sample increased after purification (Fig. 1c). This phenomenon was consistent across a wide range of settings, including different attack types (BPDA, BPDA-EOT, PGD, PGD-EOT), distance metrics (ℓ_2, ℓ_∞), and datasets (CIFAR-10 and ImageNet). This result is quite general. It is not specific to adversarial attacks and it also holds for perturbations with uniform noise (Appendix C.2).

One possible cause of this phenomenon is the large amount of noise injected by the forward diffusion process. To test this, we repeated the experiment using only the reverse process (i.e., skipping the forward noising step), and found that the increase in the ℓ_p distance remains. Furthermore, we tested an alternative sampling strategy, DDIM (Song et al., 2020a), and found similar results. These results are reported in Table 1 and S2, with additional details provided in Appendix C.1.

Table 1: Distance measurements pre/post-diffusion models on CIFAR-10 (PGD, $\ell_\infty = 8/255$).

Sampling	ℓ_2 (\downarrow)	ℓ_∞ (\downarrow)	SSIM (\uparrow)	FID (\downarrow)
DDPM	1.077 \rightarrow 3.641	0.031 \rightarrow 0.316	0.965 \rightarrow 0.796	0.226 \rightarrow 0.120
Reverse	1.149 \rightarrow 3.078	0.031 \rightarrow 0.270	0.965 \rightarrow 0.837	0.209 \rightarrow 0.183
DDIM	1.080 \rightarrow 2.810	0.031 \rightarrow 0.242	0.964 \rightarrow 0.869	0.234 \rightarrow 0.104

Diffusion-based purification leads to perceptually dissimilar outputs. While ℓ_p distances are the most widely used distance metrics (especially since adversarial attacks are typically defined within bounded ℓ_p balls), these metrics may not well capture the perceptual similarity. For example, translating an image by a single pixel can yield a large ℓ_2 difference while remaining perceptually identical. Thus, we next ask if diffusion models produce outputs that are perceptually closer to the clean image, even if ℓ_p distances increase. To investigate this, we evaluated the structural similarity index measure (SSIM) (Wang et al., 2004), a popular metric used in computer vision for quantifying perceptual similarity of images. As shown in Tables 1, we observed a substantial decrease in SSIM between purified and clean images—indicating that the outputs are not only farther away in ℓ_p space, but also perceptually more dissimilar than the initial adversarial perturbations.

Diffusion models lead to a reduction of distributional distances. We next turn to distribution-level comparisons using the Fréchet Inception Distance (FID) (Heusel et al., 2017). The FID score has been widely used to quantify the performance of generative models such as diffusion models. Here, we measure FID between the adversarial dataset and the clean dataset, both before and after

purification, to quantify whether diffusion models bring the distribution of adversarial images closer to that of the clean samples. Interestingly, we observe that purification with diffusion models leads to a reduction of the FID score between adversarial and clean distributions (Tables 1). This is consistent with the idea that diffusion models may bring the distribution of adversarial images closer to the clean data distribution Li et al. (2025); Nie et al. (2022). However, later we will show that the reduction in FID is not a reliable indicator of the robustness (see Sec. 4). For example, while DDIM achieves the largest FID reduction, it leads the lowest empirical robustness among the different samplers we tested.

Taken together, our findings challenge the “denoising” hypothesis that diffusion models improve robustness by pushing adversarial images closer to their original clean images. While diffusion models move distributions closer in high-noise regimes (App. C.2), adversarial robustness fundamentally hinges on local perturbations within a small adversarial ball, and the distributional alignment may be not sufficient.

3.2 Internal randomness dominates the behavior of diffusion models

Since diffusion models are inherently stochastic, it is important to understand how much this intrinsic noise affects the output of diffusion models. Specifically, the variability of the output of diffusion models in adversarial purification arises from two distinct sources: (i) the variability in the input images from perturbations η (causing variability around the anchor point), and (ii) the internal variability inherent to the purification system (causing variability of the anchor point).

The basic ideas are illustrated in Fig. 2. On the one hand, when fixing the input image while allowing the noise in diffusion models to vary, this variability is solely due to the internal variability of the purification system (Fig. 2a). Surprisingly, we find that this variability is quite large, as quantified by the relatively low correlations of different purification directions induced by noise (Fig. 2d; mean = 0.22 ± 0.003). On the other hand, when fixing noise in the diffusion model and allowing the input images to vary (different samples from the image neighborhood M), the variability in the output of diffusion model is solely induced by the variability in the input images (Fig. 2b; mean = 0.93 ± 0.0002). Interestingly, this variability is rather small, as demonstrated in the high correlations between the purified directions (Fig. 2e).

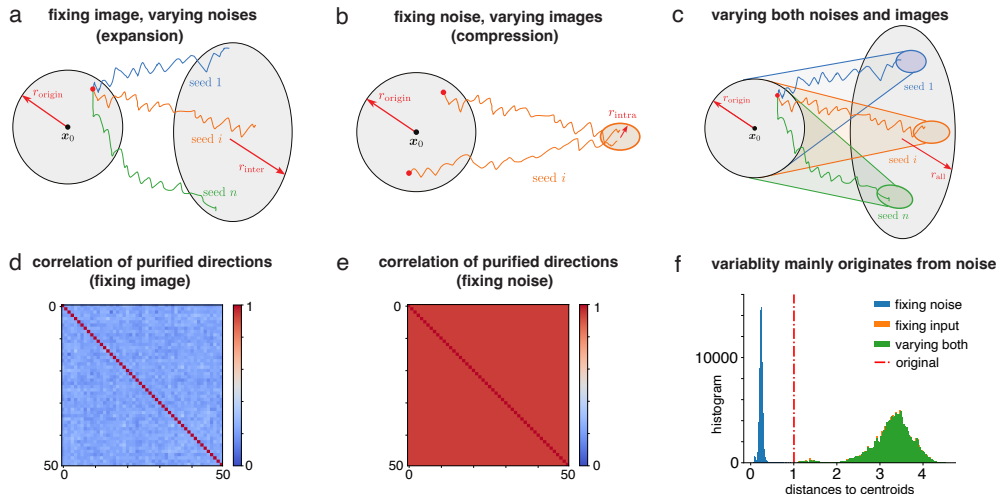


Figure 2: **The variability of the outputs of diffusion models is dominated by intrinsic noise, not variability in the input images.** (a–c) Schematics illustrating how diffusion models transform input perturbations under different sources of variability. (a) When the image is fixed and internal noise varies, purification exhibits an expansion of the input space. (b) When the noise is fixed and the image varies, the input space are compressed toward a shared direction. (c) When both image and noise vary, internal randomness dominates, producing an overall expansion. (d) Purification directions under different noise samples for the same image are weakly aligned (mean correlation: 0.22 ± 0.003). (e) Under fixed noise, purification directions across perturbed images are highly consistent (mean correlation: 0.93 ± 0.0002). (f) Distribution of ℓ_2 distances to the centroid. Fixed-noise purification compresses the input ball (radius: $1.004 \rightarrow 0.241$); varying noise leads to expansion (radius: $1.004 \rightarrow 3.282$), confirming that internal randomness drives the dominant effect.

By treating input variability as the signal and internal randomness as the noise, we define a signal-to-noise ratio (SNR) of the diffusion purification (see Appendix A for mathematical derivations):

$$\text{SNR} := \frac{\mathbb{E}_\xi [\text{Var}_{\mathbf{x}} f(\mathbf{x}|\xi)]}{\text{Var}_\xi [\mathbb{E}_{\mathbf{x}} f(\mathbf{x}|\xi)]}. \quad (7)$$

Numerically evaluating the SNR of diffusion models based on image neighborhood consistent with adversarial attack, we find the SNR is extremely low, i.e., $5.93 \pm 1.07 \times 10^{-3}$, indicating that the effect of internal stochasticity is approximately 170 times larger than that induced by input variability.

The compression effect within each randomness configuration. To investigate these effects further, we measured the ℓ_2 distances between purified samples and their respective centroids. When starting from the same clean image, internal randomness leads to an expansion effect, where the ℓ_2 radius of the perturbation space increases from 1.004 ± 0.001 to 3.282 ± 0.453 after purification. Interestingly, we observed the opposite effect when examining different inputs under a fixed randomness configuration. In this case, the purified outputs become tightly clustered, indicating a compression effect: the ℓ_2 radius shrinks to 0.241 ± 0.032 . Finally, the histogram of ℓ_2 distances shown in Fig. 2f illustrates that varying both the image and noise yields nearly the same distance distribution as varying only the noise. This further supports our conclusion that internal randomness dominates the behavior of diffusion models in adversarial purification.

4 Evaluating the robustness of diffusion models without stochasticity

The results above suggest that internal randomness in diffusion models plays a dominant role in determining the final purified output. This implies that randomness may significantly influence the empirical evaluation of adversarial robustness. In general, how to properly handle randomness in robustness evaluation has been debated (Athalye et al., 2018; Carlini et al., 2019; Gao et al., 2022; Yoon et al., 2021). In the following section, we carefully examine how randomness affects the evaluation of diffusion-based purification and its implications for interpreting robustness gains.

EOT as a transfer attack. Following the notations in Sec. 3, let L be the loss function and t be the target associated with \mathbf{x}_0 , the gradients during attack and the system during evaluation can be expressed as

$$\text{Attack: } \nabla_{\mathbf{x}} L[g(f_{\xi_{\text{attack}}}(\mathbf{x})), t], \quad \text{Test: } g(f_{\xi_{\text{test}}}(\mathbf{x})). \quad (8)$$

It is important to realize that the noise samples for calculating the attack ξ_{attack} and for the test ξ_{test} are typically different, although they are drawn from the same distribution. This means the attack is optimizing against a different function than the one will be used at test time. As a result, the attack becomes suboptimal and should be viewed as a transfer attack. This is particularly concerning in the context of diffusion models, where internal noise heavily influences the final output (as shown in the previous section). In this case, the discrepancy between $f_{\xi_{\text{attack}}}$ and $f_{\xi_{\text{test}}}$ can be substantial, limiting the attack's performance to evaluate the robustness of the purification system.

Expectation-over-transformation (EOT) (Athalye et al., 2018) was proposed to address the suboptimality introduced by stochastic gradients:

$$\text{Attack (EOT): } \mathbb{E}_\xi \nabla_{\mathbf{x}} L[g(f_{\xi_{\text{attack}}}(\mathbf{x})), t] = \nabla_{\mathbf{x}} \mathbb{E}_\xi L[g(f_{\xi_{\text{attack}}}(\mathbf{x})), t], \quad \text{Test: } g(f_{\xi_{\text{test}}}(\mathbf{x})). \quad (9)$$

Crucially, although EOT mitigates the effect of randomness in gradient computation by marginalizing over the noise during attack, randomness still remains at test time. PGD-EOT attack may be interpreted as approximately calculating the gradient of the average ensemble system $\mathbb{E}_\xi g(f_{\xi_{\text{attack}}}(\mathbf{x}))$, and later applied to the non-ensemble system $g(f_{\xi_{\text{test}}}(\mathbf{x}))$. ¹To this end, PGD-EOT can also be interpreted as a transfer attack. While EOT improves gradient quality compared to single-sample attacks (as confirmed empirically), the attack remains suboptimal. We quantify this by computing the correlation between PGD-EOT gradients and those from the optimal attack that directly targets $g(f_{\xi_{\text{test}}}(\mathbf{x}))$. We find a mean correlation of 0.1682 ± 0.0976 (see Table 5), supporting the view that PGD-EOT does not fully capture the optimal gradients of the defense system.

¹For this approximation to be exact, the expectation operation needs to commute with the loss function L . This in general does not hold for cross-entropy loss, but was not explicitly discussed in Athalye et al. (2018).

Here we propose an alternative evaluation method by fixing the randomness during both attack generation and testing—specifically, setting $\xi_{\text{attack}} = \xi_{\text{test}}$. This approach eliminates the mismatch in stochasticity between the attack and defense, thereby addressing concerns related to suboptimal gradients and transfer attacks. It enables a more faithful estimation of the robustness of adversarial purification systems independent of randomness. As we will demonstrate below, even under fully controlled randomness, diffusion models still exhibit non-trivial robustness, although the observed robust accuracy is significantly lower than previous reports.

Table 2: Robustness of diffusion models w/o. stochasticity on CIFAR-10 ($\ell_{\infty} = 8/255$, $t = 100$).

Model	Fix Random	Clean Acc.	PGD	PGD-EOT
DDPM	✗	86.0 \pm 0.8%	71.9 \pm 0.2%	59.3%
	✓	85.8 \pm 0.4%	23.7\pm0.7%	—

Table 3: Robustness of diffusion models w/o. stochasticity on ImageNet ($\ell_{\infty} = 4/255$, $t = 150$).

Model	Fix Random	Clean Acc.	BPDA	BPDA-EOT
Guided	✗	67.2 \pm 2.4%	63.7 \pm 1.2%	59.0%
	✓	68.5 \pm 0.8%	29.5\pm0.4%	—

Robustness of diffusion models without stochasticity. Previous work (Nie et al., 2022) reported that using a diffusion timestep of $t = 100$ resulted in approximately 70% robust accuracy on CIFAR-10. Subsequent evaluations reduced this estimate to around 46% by applying stronger PGD-EOT attacks with more steps and samples (Lee & Kim, 2023; Li et al., 2025). In our study, we control for the internal randomness of diffusion models by fixing random seeds in both the forward and reverse processes (see Appendix B for implementation details). After removing the effects of stochasticity, we find that the actual robustness gain of diffusion models on CIFAR-10 drops to **23.7%** under PGD attacks. On ImageNet, using BPDA with fixed randomness yields a robust accuracy of **29.5%**.² These results are substantially lower than previously reported robustness estimates (see Tables 2 and 3). Importantly, controlling randomness does not affect the clean accuracy of the models.

Table 4: Transfer attack across different random configurations.

Dataset	Fix Random	PGD/BPDA
CIFAR-10	✓	77.4 \pm 0.36%
ImageNet	✓	66.3 \pm 2.32%

Table 5: Correlations between PGD/EOT attacks on CIFAR-10.

Attacks	Correlation
PGD (Fix) vs. PGD (Fix)	0.0818 \pm 0.0709
PGD-EOT vs. PGD (Fix)	0.1682 \pm 0.0976

Transfer attack across random configurations. We further conduct transfer attack experiments to illustrate how randomness effect robustness evaluation. We calculated the attack with a fixed randomness configuration, and evaluated with a different fixed randomness configuration. Based on our theoretical reasoning above, we hypothesize that should mimic the effect of not controlling randomness. In support of our hypothesis, the observed empirical robustness accuracies for both CIFAR-10 and ImageNet are generally consistent with those reported using reported previously (Table 4). Additionally, we measure the correlation between the adversarial perturbations generated under different random configurations and find a mean correlation of 0.0818 ± 0.0709 (Table 5).

5 Diffusion models improve robustness by compressing image space

We finally address the key question of how diffusion models lead to non-trivial robustness even when randomness is fixed. An important clue comes from the compression effect observed in Sec. 3.2. Specifically, after transformation by the diffusion model, the average distance from samples to their centroid drops to about 0.2-0.3, compared to around 1.0 in the original neighbourhood. Under our mathematical formulation, this indicates the Jacobian of the diffusion models at the clean image tends to compress the image space. To test this, we evaluated the singular value spectrum of the Jacobian with 50 samples on CIFAR-10, and found that over 90% of the singular values are smaller than 0.25, with only 1.3% exceed 1.0 (Fig. 3a).

²We were unable to compute full PGD gradients for diffusion models on ImageNet.

To quantify the magnitude of compression, we define a simple scalar measure which we will refer to as the compression rate:

$$\alpha_{f_\xi}(\mathbf{x}, \mathbf{x}_0) = \frac{\|f_\xi(\mathbf{x}) - f_\xi(\mathbf{x}_0)\|}{\|\mathbf{x} - \mathbf{x}_0\|} \approx \|J_{f_\xi}(\mathbf{x}_0)\boldsymbol{\eta}\|. \quad (10)$$

The compression rate above is defined for a given clean image \mathbf{x} and a sample \mathbf{x}_0 from its neighborhood. One can estimate the average compression rate for a given clean image by sampling many images from its neighborhood and then performing averaging. We can further compute the compression rate of a dataset under a given diffusion model by averaging the compression rate over images. Importantly, the compression rate is easy to compute and does not involve gradients.

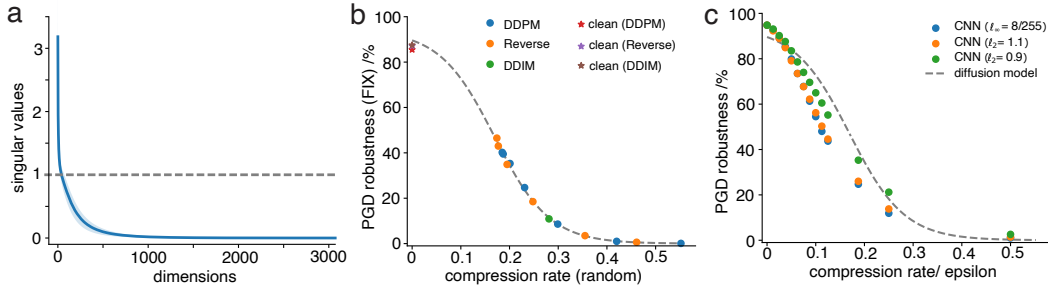


Figure 3: Diffusion models improve robustness by compressing image space. (a) The singular value spectrum of Jacobian matrices shows that diffusion models strongly compress input space: over 90% of singular values are below 0.25, and only 1.3% exceed 1.0. (b) The compression rate and robustness without stochasticity of diffusion models follow a consistent relation well captured by a sigmoid function. Note that the curve generalizes across different sampling methods and extrapolates smoothly to clean accuracies at the y-intercept. (c) The compression–robustness curve resembles the PGD robustness curve of the base classifier under smaller attack budgets.

Lawful relation between compression rate and adversarial robustness. Adversarial examples arise when a small neighborhood around a clean image intersects a classifier’s decision boundary. We reason that the compression of image space effectively reduces the size of image neighborhood and thus reduces the odds of the transformed neighborhood \tilde{M}_ξ intersecting with a decision boundary. This predicts a direct relationship between the compression rate and adversarial robustness.

We test this prediction using CIFAR-10. We take advantage of the fact that different implementations of diffusion models (DDPM, Reverse-only, DDIM) lead to different adversarial robustness (see Table 6). Examining a collection of diffusion models with various hyper-parameters (Table 7), we plot their robustness performances against their compression rates. Strikingly, we find that the two quantities exhibit a lawful relationship (see Fig. 3b). The compression-robustness curve increases sharply for a compression rate around 0.2. We find that the relation between compression and robustness can be well fitted by a sigmoidal function. Interestingly, extrapolating the fitted curve to zero compression rate lead to relatively accurate prediction of the clean accuracy.

Our results suggest a way to find parameter settings that may lead to higher robustness, i.e., by searching for regimes with lower compression rate. Importantly, compression rate is very easy to estimate computationally, with no need of gradient computation. We find the reverse-only model leads to lower compression rate than DDPM (Table 6). Consistent with our theory, the robustness for reverse-only models are generally higher than that of DDPM. When increasing the number of diffusion timesteps beyond what was typically used in prior studies $t = 100$ to $t = 200$, we find that the compression rate of reverse-only model is further decreased. This setting also results in a higher robustness of **46.5%**. Interestingly, further increasing the timestep to 300 leads to worse compression and worse adversarial robustness. We note that, for $t = 300$, the robustness obtained is slightly higher than the prediction of our fitted sigmoid curve (not shown in Fig. 3b). We reason this mismatch comes from two potentials: (i) the robustness improvement is constrained by the drop of the clean accuracy (see Appendix C.4 for the effect of timesteps); (ii) gradient masking, both due to large number of timesteps. Therefore we did not investigate even longer timesteps.

We further consider alternative predictors of the robustness. First, we find that, the averaged magnitude of adversarial attack found by the PGD attacks is not a reliable predictor of the robustness of a method (Table 6), although it is informative for whether the attack on a particular image would be successful. Second, the FID score (as mentioned earlier) is also a poor indicator of the robustness of a method.

The sigmoid relation resembles the robustness curve of base classifier. The observed sigmoid relationship between compression rate and robustness suggests a more fundamental explanation. Building on our compression-based theory, we hypothesize that this pattern reflects the intrinsic relationship between attack budget and adversarial robustness. This theory implies that the robustness of a base CNN classifier should also follow a sigmoid curve when subjected to attacks with decreasing budgets. To test this, we perform PGD attacks on the base classifier using progressively smaller budgets (decaying corresponding to the measured compression rates). We find that the CNN classifier exhibits a similar robustness curve under different attacks (Fig. 3c). The robustness curves align in range, but not perfectly in shape, likely due to differences between the adversarial regions around the original and anchor points. Nonetheless, these results provide additional support for our theory: the compression effect of diffusion models reduces the effective attack budget, thereby improving robustness in a predictable, theoretically grounded manner.

Table 6: Compression rates and adversarial robustness on CIFAR-10.

Sampling	Compression rate			Adversarial	
	PGD (Robust)	PGD (Non-robust)	Uniform	PGD (Fix)	
DDPM	0.798 ± 0.124	0.989 ± 0.201	0.231 ± 0.046	23.7%	
Reverse	0.738 ± 0.106	0.864 ± 0.151	0.195 ± 0.046	34.9%	
DDIM	0.717 ± 0.119	0.815 ± 0.140	0.281 ± 0.048	10.9%	

Table 7: The effect of diffusion timesteps on CIFAR-10.

Model		$t = 10$	$t = 20$	$t = 50$	$t = 100$	$t = 150$	$t = 200$	$t = 300$
DDPM	Compress	0.552	0.420	0.299	0.231	0.201	0.187	0.185
	PGD (Fix)	0.1%	1.0%	8.6%	23.7%	35.3%	39.5%	40.2%
Reverse	Compress	0.461	0.355	0.248	0.195	0.177	0.174	0.200
	PGD (Fix)	0.6%	3.5%	18.5%	34.9%	43.0%	46.5%	42.6%

6 Discussions

We have conducted a systematic analysis of how diffusion models improve adversarial robustness. Contrary to the common intuition that purification brings inputs closer to clean data, we find that diffusion models tend to push perturbed images away from the clean samples. This motivates our use of the term “anchor points” to describe the purified outputs corresponding to clean images. While this push-away effect can reduce clean accuracy, the anchor points still support high classification performance, which is an essential requirement for any effective purification system. Simultaneously, diffusion models exhibit a strong compression of the image space around the anchor points. It is this compression effect that underlies the robustness improvements offered by diffusion-based purification. We find that the previously reported robustness gains consist of two components: (i) failure of the attack due to suboptimal gradient estimation caused by randomness, and (ii) *bona fide* robustness improvement arising from the compression of image space. By aligning the randomness during attacking and testing, we isolate the latter effect and show that while the robustness gain is significantly lower than prior reports, there are still non-trivial robustness improvements unrelated to stochasticity. Crucially, we find that the robustness gain without stochasticity correlates strongly with the compression rate across different diffusion sampling methods, forming a consistent and lawful relationship. This provides strong support for our theory. Our results point to a promising direction for designing “compression-based purification”, which hinges on two criteria: (i) high clean accuracy at anchor points, and (ii) strong compression rates around anchor points. Systems meeting these criteria should achieve reliable adversarial robustness without relying on stochasticity.

Limitations This study has several limitations. First, due to limited computational resources, we were unable to perform full gradient-based attacks on ImageNet. The EOT-based evaluation we conducted is based on relatively small number of samples. Second, when the number of diffusion timesteps is large, issues such as gradient explosion or vanishing may occur—even with fixed noise—potentially leading to gradient masking. We suspect that for $t = 300$ (Table 7), the robustness of the Reverse model maybe contaminated by inaccuracy of gradient calculations. Finally, although we identified that reverse-only diffusion models offer better robustness gains, we did not design a new purification system in this work. Developing such a system based on our compression theory is beyond the current scope and remains an exciting direction for future research.

References

Anish Athalye, Nicholas Carlini, and David Wagner. Obfuscated gradients give a false sense of security: Circumventing defenses to adversarial examples. In *International conference on machine learning*, pp. 274–283. PMLR, 2018.

Nicholas Carlini, Anish Athalye, Nicolas Papernot, Wieland Brendel, Jonas Rauber, Dimitris Tsipras, Ian Goodfellow, Aleksander Madry, and Alexey Kurakin. On evaluating adversarial robustness. *arXiv preprint arXiv:1902.06705*, 2019.

Nicholas Carlini, Florian Tramer, Krishnamurthy Dj Dvijotham, Leslie Rice, Mingjie Sun, and J Zico Kolter. (certified!!) adversarial robustness for free! *arXiv preprint arXiv:2206.10550*, 2022.

Jeremy Cohen, Elan Rosenfeld, and Zico Kolter. Certified adversarial robustness via randomized smoothing. In *international conference on machine learning*, pp. 1310–1320. PMLR, 2019.

Francesco Croce and Matthias Hein. Reliable evaluation of adversarial robustness with an ensemble of diverse parameter-free attacks. In *International conference on machine learning*, pp. 2206–2216. PMLR, 2020.

Francesco Croce, Maksym Andriushchenko, Vikash Sehwag, Edoardo Debenedetti, Nicolas Flammarion, Mung Chiang, Prateek Mittal, and Matthias Hein. Robustbench: a standardized adversarial robustness benchmark. *arXiv preprint arXiv:2010.09670*, 2020.

Jia Deng, Wei Dong, Richard Socher, Li-Jia Li, Kai Li, and Li Fei-Fei. Imagenet: A large-scale hierarchical image database. In *2009 IEEE conference on computer vision and pattern recognition*, pp. 248–255. Ieee, 2009.

Prafulla Dhariwal and Alexander Nichol. Diffusion models beat gans on image synthesis. *Advances in neural information processing systems*, 34:8780–8794, 2021.

Gavin Weiguang Ding, Luyu Wang, and Xiaomeng Jin. AdverTorch v0.1: An adversarial robustness toolbox based on pytorch. *arXiv preprint arXiv:1902.07623*, 2019.

Nic Ford, Justin Gilmer, Nicolas Carlini, and Dogus Cubuk. Adversarial examples are a natural consequence of test error in noise. *arXiv preprint arXiv:1901.10513*, 2019.

Yue Gao, Ilia Shumailov, Kassem Fawaz, and Nicolas Papernot. On the limitations of stochastic pre-processing defenses. *Advances in Neural Information Processing Systems*, 35:24280–24294, 2022.

Ian J Goodfellow, Jonathon Shlens, and Christian Szegedy. Explaining and harnessing adversarial examples. *arXiv preprint arXiv:1412.6572*, 2014.

Shixiang Gu and Luca Rigazio. Towards deep neural network architectures robust to adversarial examples. *arXiv preprint arXiv:1412.5068*, 2014.

Martin Heusel, Hubert Ramsauer, Thomas Unterthiner, Bernhard Nessler, and Sepp Hochreiter. Gans trained by a two time-scale update rule converge to a local nash equilibrium. *Advances in neural information processing systems*, 30, 2017.

Jonathan Ho, Ajay Jain, and Pieter Abbeel. Denoising diffusion probabilistic models. *Advances in neural information processing systems*, 33:6840–6851, 2020.

Yifei Huang, Yaodong Yu, Hongyang Zhang, Yi Ma, and Yuan Yao. Adversarial robustness of stabilized neural ode might be from obfuscated gradients. In Joan Bruna, Jan Hesthaven, and Lenka Zdeborova (eds.), *Proceedings of the 2nd Mathematical and Scientific Machine Learning Conference*, volume 145 of *Proceedings of Machine Learning Research*, pp. 497–515. PMLR, 16–19 Aug 2022.

Zahra Kadkhodaie, Florentin Guth, Eero P Simoncelli, and Stéphane Mallat. Generalization in diffusion models arises from geometry-adaptive harmonic representations. In *The Twelfth International Conference on Learning Representations*, 2024.

Alex Krizhevsky and Geoffrey Hinton. Learning multiple layers of features from tiny images. Technical report, University of Toronto, 2009.

Minjong Lee and Dongwoo Kim. Robust evaluation of diffusion-based adversarial purification. In *Proceedings of the IEEE/CVF International Conference on Computer Vision*, pp. 134–144, 2023.

Xiao Li, Wenxuan Sun, Huanran Chen, Qiongxu Li, Yining Liu, Yingzhe He, Jie Shi, and Xiaolin Hu. Adbm: Adversarial diffusion bridge model for reliable adversarial purification. *International Conference on Learning Representations*, 2025.

Fangzhou Liao, Ming Liang, Yinpeng Dong, Tianyu Pang, Xiaolin Hu, and Jun Zhu. Defense against adversarial attacks using high-level representation guided denoiser. In *Proceedings of the IEEE conference on computer vision and pattern recognition*, pp. 1778–1787, 2018.

Guang Lin, Zerui Tao, Jianhai Zhang, Toshihisa Tanaka, and Qibin Zhao. Robust diffusion models for adversarial purification. *arXiv preprint arXiv:2403.16067*, 2024.

Aleksander Madry, Aleksandar Makelov, Ludwig Schmidt, Dimitris Tsipras, and Adrian Vladu. Towards deep learning models resistant to adversarial attacks. *arXiv preprint arXiv:1706.06083*, 2017.

Weili Nie, Brandon Guo, Yujia Huang, Chaowei Xiao, Arash Vahdat, and Animashree Anandkumar. Diffusion models for adversarial purification. In *International Conference on Machine Learning*, pp. 16805–16827. PMLR, 2022.

Tianyu Pang, Xiao Yang, Yinpeng Dong, Hang Su, and Jun Zhu. Bag of tricks for adversarial training. In *International Conference on Learning Representations*, 2020.

Nicolas Papernot, Patrick McDaniel, Ian Goodfellow, Somesh Jha, Z Berkay Celik, and Ananthram Swami. Practical black-box attacks against machine learning. In *Proceedings of the 2017 ACM on Asia conference on computer and communications security*, pp. 506–519, 2017.

Jonas Rauber, Roland Zimmermann, Matthias Bethge, and Wieland Brendel. Foolbox native: Fast adversarial attacks to benchmark the robustness of machine learning models in pytorch, tensorflow, and jax. *Journal of Open Source Software*, 5(53):2607, 2020. doi: 10.21105/joss.02607. URL <https://doi.org/10.21105/joss.02607>.

Hadi Salman, Mingjie Sun, Greg Yang, Ashish Kapoor, and J Zico Kolter. Denoised smoothing: A provable defense for pretrained classifiers. *Advances in Neural Information Processing Systems*, 33:21945–21957, 2020.

Pouya Samangouei, Maya Kabkab, and Rama Chellappa. Defense-gan: Protecting classifiers against adversarial attacks using generative models. In *International Conference on Learning Representations*, 2018.

Lukas Schott, Jonas Rauber, Matthias Bethge, and Wieland Brendel. Towards the first adversarially robust neural network model on mnist. *arXiv preprint arXiv:1805.09190*, 2018.

Maximilian Seitzer. pytorch-fid: FID Score for PyTorch. <https://github.com/mseitzer/pytorch-fid>, August 2020. Version 0.3.0.

Ali Shafahi, Mahyar Najibi, Mohammad Amin Ghiasi, Zheng Xu, John Dickerson, Christoph Studer, Larry S Davis, Gavin Taylor, and Tom Goldstein. Adversarial training for free! *Advances in Neural Information Processing Systems*, 32, 2019.

Changhao Shi, Chester Holtz, and Gal Mishne. Online adversarial purification based on self-supervision. *arXiv preprint arXiv:2101.09387*, 2021.

Jiaming Song, Chenlin Meng, and Stefano Ermon. Denoising diffusion implicit models. In *International Conference on Learning Representations*, 2020a.

Yang Song, Taesup Kim, Sebastian Nowozin, Stefano Ermon, and Nate Kushman. Pixeldefend: Leveraging generative models to understand and defend against adversarial examples. In *International Conference on Learning Representations*, 2018.

Yang Song, Jascha Sohl-Dickstein, Diederik P Kingma, Abhishek Kumar, Stefano Ermon, and Ben Poole. Score-based generative modeling through stochastic differential equations. In *International Conference on Learning Representations*, 2020b.

Jiachen Sun, Jiongxiao Wang, Weili Nie, Zhiding Yu, Zhuoqing Mao, and Chaowei Xiao. A critical revisit of adversarial robustness in 3d point cloud recognition with diffusion-driven purification. 2023.

Christian Szegedy, Wojciech Zaremba, Ilya Sutskever, Joan Bruna, Dumitru Erhan, Ian Goodfellow, and Rob Fergus. Intriguing properties of neural networks. *arXiv preprint arXiv:1312.6199*, 2013.

Florian Tramèr, Alexey Kurakin, Nicolas Papernot, Ian Goodfellow, Dan Boneh, and Patrick McDaniel. Ensemble adversarial training: Attacks and defenses. In *International Conference on Learning Representations*, volume 1, pp. 2, 2018.

Jinyi Wang, Zhaoyang Lyu, Dahua Lin, Bo Dai, and Hongfei Fu. Guided diffusion model for adversarial purification. *arXiv preprint arXiv:2205.14969*, 2022.

Yisen Wang, Xingjun Ma, James Bailey, Jinfeng Yi, Bowen Zhou, and Quanquan Gu. On the convergence and robustness of adversarial training. *arXiv preprint arXiv:2112.08304*, 2021.

Zhou Wang, Alan C Bovik, Hamid R Sheikh, and Eero P Simoncelli. Image quality assessment: from error visibility to structural similarity. *IEEE transactions on image processing*, 13(4):600–612, 2004.

Shutong Wu, Jiongxiao Wang, Wei Ping, Weili Nie, and Chaowei Xiao. Defending against adversarial audio via diffusion model. In *The Eleventh International Conference on Learning Representations*, 2022.

Chaowei Xiao, Zhongzhu Chen, Kun Jin, Jiongxiao Wang, Weili Nie, Mingyan Liu, Anima Anandkumar, Bo Li, and Dawn Song. Densepure: Understanding diffusion models for adversarial robustness. In *The Eleventh International Conference on Learning Representations, ICLR 2023, Kigali, Rwanda, May 1-5, 2023*, 2023.

Dong Yin, Raphael Gontijo Lopes, Jon Shlens, Ekin Dogus Cubuk, and Justin Gilmer. A fourier perspective on model robustness in computer vision. *Advances in Neural Information Processing Systems*, 32, 2019.

Jongmin Yoon, Sung Ju Hwang, and Juho Lee. Adversarial purification with score-based generative models. In *International Conference on Machine Learning*, pp. 12062–12072. PMLR, 2021.

A Variance decomposition in diffusion models for adversarial purification

Following the notation in Sec. 3, we write the output of diffusion models as $f(\mathbf{x}, \xi)$. The input variability comes from image perturbations, $\mathbf{x} = \mathbf{x}_0 + \epsilon \boldsymbol{\eta}$. The internal randomness is captured by ξ .

Assume inputs \mathbf{x} are independent with randomness ξ , the total variance of diffusion models can then be decomposed as

$$\text{Var}_{\mathbf{x}, \xi}[f(\mathbf{x}, \xi)] = \mathbb{E}_\xi [\text{Var}_{\mathbf{x}} f(\mathbf{x}|\xi)] + \text{Var}_\xi [\mathbb{E}_{\mathbf{x}} f(\mathbf{x}|\xi)]. \quad (11)$$

The result directly follows the law of total variance. Here we append the proof for completeness.

Proof. Define the following means

$$\begin{aligned} \mu_\xi &:= \mathbb{E}_{\mathbf{x}} f(\mathbf{x}|\xi) \quad (\text{mean at fixed randomness } \xi) \\ \mu &:= \mathbb{E}_{\mathbf{x}, \xi} f(\mathbf{x}, \xi) = \mathbb{E}_\xi \mu_\xi \quad (\text{global mean}). \end{aligned}$$

Expand the total variance

$$\text{Var}_{\mathbf{x}, \xi}[f(\mathbf{x}, \xi)] = \mathbb{E}_{\mathbf{x}, \xi} [\|f(\mathbf{x}, \xi) - \mu\|^2] = \mathbb{E}_\xi [\mathbb{E}_{\mathbf{x}} [\|f(\mathbf{x}, \xi) - \mu\|^2]].$$

Now insert and subtract μ_ξ inside the norm:

$$\begin{aligned} \|f(\mathbf{x}, \xi) - \mu\|^2 &= \|f(\mathbf{x}, \xi) - \mu_\xi + \mu_\xi - \mu\|^2 \\ &= \|f(\mathbf{x}, \xi) - \mu_\xi\|^2 + 2\langle f(\mathbf{x}, \xi) - \mu_\xi, \mu_\xi - \mu \rangle + \|\mu_\xi - \mu\|^2. \end{aligned}$$

Taking expectation over \mathbf{x} (for fixed ξ), the cross term vanishes:

$$\mathbb{E}_{\mathbf{x}}[f(\mathbf{x}, \xi) - \mu_\xi] = 0 \quad \Rightarrow \quad \mathbb{E}_{\mathbf{x}} [\langle f(\mathbf{x}, \xi) - \mu_\xi, \mu_\xi - \mu \rangle] = 0.$$

Therefore

$$\mathbb{E}_{\mathbf{x}} [\|f(\mathbf{x}, \xi) - \mu\|^2] = \mathbb{E}_{\mathbf{x}} [\|f(\mathbf{x}, \xi) - \mu_\xi\|^2] + \|\mu_\xi - \mu\|^2.$$

Finally take expectation over ξ :

$$\begin{aligned} \text{Var}_{\mathbf{x}, \xi}[f(\mathbf{x}, \xi)] &= \mathbb{E}_\xi [\mathbb{E}_{\mathbf{x}} [\|f(\mathbf{x}, \xi) - \mu_\xi\|^2]] + \mathbb{E}_\xi [\|\mu_\xi - \mu\|^2] \\ &= \mathbb{E}_\xi [\text{Var}_{\mathbf{x}} f(\mathbf{x}|\xi)] + \text{Var}_\xi [\mathbb{E}_{\mathbf{x}} f(\mathbf{x}|\xi)]. \end{aligned}$$

This completes the proof of the decomposition. \square

Based on the decomposition, the first term $\mathbb{E}_\xi [\text{Var}_{\mathbf{x}} f(\mathbf{x}|\xi)]$ represents the input variability, and the second term $\text{Var}_\xi [\mathbb{E}_{\mathbf{x}} f(\mathbf{x}|\xi)]$ represents the internal variability. Treating the input perturbations as signals and internal randomness as noise, we can further define the SNR in eq. 7.

B Implementation details of adversarial attacks on diffusion models

Datasets and base classifiers The experiments were conducted on the CIFAR-10 Krizhevsky & Hinton (2009) and ImageNet (Deng et al., 2009) datasets. For CIFAR-10, we subsampled the first 1000 images from the test set. For ImageNet, we subsampled the first 200 images from the validation set. Standard preprocessing was applied to the datasets. We used the standard classifiers from the RobustBench (Croce et al., 2020)<https://github.com/RobustBench/robustbench>. Namely, the WideResNet-28-10 model for CIFAR-10, and ResNet-50 model for ImageNet. The clean accuracy on our subsampled set for the classifier is 94.8% on CIFAR-10 (vs. 94.78% on the full set) and 74.5% on ImageNet (vs. 76.52% on the full set).

Diffusion models We focused on discrete-time diffusion models in this paper to avoid the potential gradient masking induced by numerical solvers in continuous-time models (Huang et al., 2022). For CIFAR-10, we used the official checkpoint of DDPM (converted to PyTorch from Tensorflow https://github.com/pesser/pytorch_diffusion) instead of Score-SDE. For ImageNet, we used the official checkpoint of 256×256 unconditional Guided diffusion (Dhariwal & Nichol, 2021) <https://github.com/openai/guided-diffusion> as the purification system. The purification time steps were kept the same with Nie et al. (2022), namely $t^* = 0.1$ (100 forward and 100 reverse steps) for CIFAR-10 and $t^* = 0.15$ (150 forward and 150 reverse steps) for ImageNet.

The DiffPure (Nie et al., 2022) framework proposed to utilize both the forward and reverse processes of diffusion models for adversarial purification. Since the forward process introduces a large amount of randomness, we explore whether it's possible to remove the forward process, thus only using the reverse process of diffusion models for adversarial purification. A similar reverse-only framework was proposed in DensePure (Xiao et al., 2023), but further equipped with a majority voting mechanism to study the certificated robustness.

Fixing randomness in diffusion models We controlled the randomness within diffusion models by controlling the random seeds during both the forward and reverse processes. For the base seed s , i -th batch of data at the t step of the forward/reverse process, we set the random seed

$$\text{seed}(s, i, t) = \begin{cases} \text{hash}(s, i, 2t), & \text{if forward process} \\ \text{hash}(s, i, 2t + 1), & \text{if reverse process} \end{cases} \quad (12)$$

before sampling the Gaussian noise from eq. 1 or eq. 2. The multiplicative hashing function

$$\text{hash}(s, i, t) = (p_s \cdot s) \oplus (p_i \cdot i) \oplus (p_t \cdot t) \mod 2^{32} \quad (13)$$

where p_s, p_i, p_t are large numbers coprime with each other to avoid collision and \oplus denotes bitwise XOR. This setting ensures that we have a different random seed for each batch of data and timesteps in the forward/reverse process, but will keep the randomness the same through the entire purification process if encountering the same data batch.

Adversarial attacks We conducted BPDA/BPDA-EOT and PGD/PGD-EOT attacks (Athalye et al., 2018) on CIFAR-10 with $\ell_\infty = 8/255$, and BPDA/BPDA-EOT attacks on ImageNet with $\ell_\infty = 4/255$. The PGD was conducted based on the foolbox (Rauber et al., 2020)<https://github.com/bethgelab/foolbox>, and the BPDA wrapper was adapted from advertorch (Ding et al., 2019)<https://github.com/BorealisAI/advertorch>. Full gradients were calculated for the PGD/PGD-EOT as Lee & Kim (2023) discovered that the approximations methods used in the original DiffPure (Nie et al., 2022) incurred weaker attacks. The full gradient of PGD/PGD-EOT is the strongest attack for DiffPure methods according to Lee & Kim (2023) experiments, and is very computationally expensive. We ran our CIFAR-10 attack experiments on a NVIDIA RTX 6000 GPU for 10 days. We were not able to conduct the full PGD attack on ImageNet in a reasonable time given our available resources. The key hyperparameters for our attacks are listed in Table S1. All attacks were repeated three times ($n = 3$) to compute the standard deviation, except for the EOT experiments, for which we were unable to do so due to limited computational resources. We used the base seeds $s = 0, 1, 2$ for all experiments.

FID score The FID score was calculated based on the `pytorch-fid` package (Seitzer, 2020)<https://github.com/mseitzer/411pytorch-fid>. We compute the FID score using 768-dimensional pre-classifier features due to the limited number of PGD samples .

Table S1: Hyperparameters for adversarial attacks.

Hyperparameters	Values {CIFAR-10, ImageNet}
Attack magnitude	{8, 4} / 255
PGD steps	40
Relative PGD step size	0.01 / 0.3
EOT numbers	15
Batch size	1
Random factor p_s	83492791
Random factor p_i	73856093
Random factor p_t	19349663

C Additional experimental results

C.1 ℓ_p distance measurements during DiffPure

Additional distance measurements during the DiffPure process are shown in Fig. S1 and S2. For CIFAR-10, we further measured the ℓ_∞ distances for the experiment illustrated in Fig. 1c. For ImageNet, we repeated the same experiment with the unconditional Guided diffusion with 150 diffusion and denoising steps ($t^* = 0.15$, the same setting with the DiffPure (Nie et al., 2022)), and measured the ℓ_2/ℓ_∞ distances. The distances during the intermediate diffusion process in ImageNet (Fig. S2) are not shown as the code base implemented the one-step diffusion equation equivalent to the multistep diffusion. Again, similar effects were observed under both ℓ_2/ℓ_∞ distances across datasets, namely, diffusion models purified to states further away from the clean images, considerably larger than the original adversarial perturbation ball. Detailed data points are listed in Table S3,S4,S2. Specifically, the ℓ_2/ℓ_∞ distances to clean samples at the init point ($t = 0$, the scale of the original perturbation), maximum point ($t = 100/150$, after forward diffusion), and end point ($t = 200/300$, after the reverse denoising). The end point distances are roughly 4 or 5 times of the size of the adversarial ball under ℓ_2 distance on CIFAR-10/ImageNet, and 10 or 26 times under ℓ_∞ distance. Diffusion models transit back to the ℓ_2 shrinkage regime beyond the uniform noise of $\epsilon = 16/255$, which is twice of the standard ℓ_∞ adversarial ball considered for CIFAR-10.

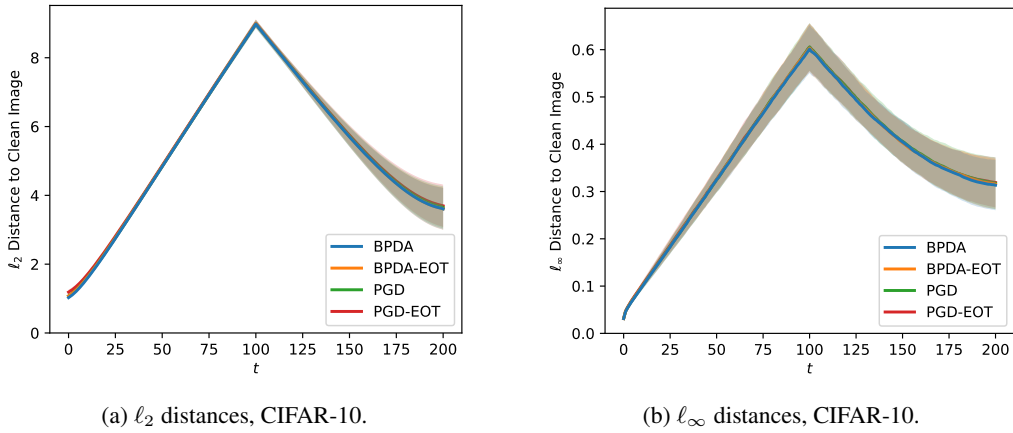


Figure S1: Additional distance measurements during DiffPure on CIFAR-10.

C.2 Behavior of diffusion models under random perturbations

We wonder if the behavior of adversarial attacks under diffusion models is special at all, that is, whether the push-away phenomena we observed are in fact general to arbitrary perturbations around the clean images. To test this, we generated perturbations of clean images by sampling random noise uniformly with a fixed magnitude. We first tested small perturbations that match the size of the adversarial attack on CIFAR-10 ($\ell_\infty = 8/255$ uniform noise). We found that the behavior of the

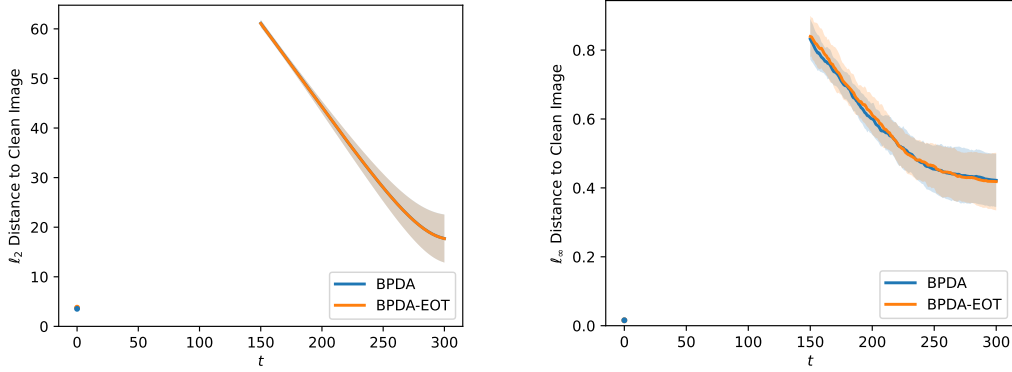
(a) ℓ_2 distances, ImageNet.(b) ℓ_∞ distances, ImageNet.

Figure S2: Additional distance measurements during DiffPure on ImageNet.

Table S2: ℓ_2/ℓ_∞ distances measurements during DiffPure on ImageNet ($\ell_\infty = 4/255$).

Distances	Attack	Init ($t = 0$)	Max ($t = 150$)	End ($t = 300$)
ℓ_2	BPDA	3.537 ± 0.079	61.116 ± 0.738	17.712 ± 4.851
	BPDA-EOT	3.772 ± 0.139	61.078 ± 0.762	17.694 ± 4.838
ℓ_∞	BPDA	0.016 ± 0.000	0.832 ± 0.059	0.422 ± 0.077
	BPDA-EOT	0.016 ± 0.000	0.839 ± 0.060	0.418 ± 0.084

model under random noise (Fig. S3a, blue curve) is almost identical to that induced by adversarial attack (Fig. 1c, blue curve). These results, together with those reported above, suggest that diffusion models are not able to reduce the distances to a clean image from a slightly perturbed clean image. This raised the intriguing possibility that the clean images do not reside on the local peaks of the image priors learned in the diffusion models. This may make sense given the in memorization v.s. generalization trade-off (Kadkhodaie et al., 2024). That is, a model simply encodes every clean image as the prior mode may not generalize well.

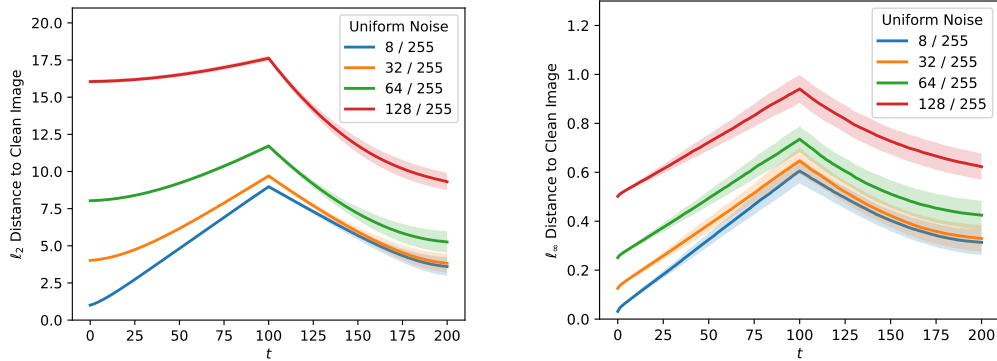
(a) ℓ_2 distances, uniform noises.(b) ℓ_∞ distances, uniform noises.

Figure S3: Distance measurements under random perturbations on CIFAR-10.

Although the results above indicate that diffusion models are ineffective in removing small perturbations, it is possible that they may be more effective in removing noise induced by larger perturbations. We performed the same ℓ_2 distance analysis using three larger levels of uniform noises, ranging from $\epsilon = \{32, 64, 128\}/255$, to examine the model behavior under larger perturbations. As the noise level increases, the ℓ_2 distances of the final purified states increase. Interestingly, the model transits from “pushing-away” to “shrinkage” under very large perturbations.

Table S3: ℓ_2 distance measurements during DiffPure on CIFAR-10 ($\ell_\infty = 8/255$).

Attack	Init ($t = 0$)	Max ($t = 100$)	End ($t = 200$)
BPDA	1.027 ± 0.023	8.976 ± 0.118	3.606 ± 0.607
BPDA-EOT	1.072 ± 0.046	8.992 ± 0.116	3.607 ± 0.615
PGD (Full)	1.077 ± 0.040	8.980 ± 0.118	3.646 ± 0.614
PGD-EOT	1.188 ± 0.072	8.999 ± 0.115	3.695 ± 0.617
Uniform ($\epsilon = 8/255$)	1.004 ± 0.009	8.979 ± 0.113	3.598 ± 0.618
Uniform ($\epsilon = 16/255$)	4.015 ± 0.034	9.699 ± 0.124	3.823 ± 0.640
Uniform ($\epsilon = 32/255$)	8.030 ± 0.065	11.715 ± 0.145	5.258 ± 0.714
Uniform ($\epsilon = 128/255$)	16.051 ± 0.129	17.622 ± 0.184	9.307 ± 0.581

Table S4: ℓ_∞ distance measurements during DiffPure on CIFAR-10 ($\ell_\infty = 8/255$).

Attack	Init ($t = 0$)	Max ($t = 100$)	End ($t = 200$)
BPDA	0.031 ± 0.000	0.601 ± 0.051	0.313 ± 0.053
BPDA-EOT	0.031 ± 0.000	0.603 ± 0.051	0.316 ± 0.053
PGD (Full)	0.031 ± 0.000	0.606 ± 0.050	0.317 ± 0.055
PGD-EOT	0.031 ± 0.000	0.606 ± 0.050	0.319 ± 0.053
Uniform ($\epsilon = 8/255$)	0.031 ± 0.000	0.605 ± 0.050	0.314 ± 0.052
Uniform ($\epsilon = 16/255$)	0.125 ± 0.000	0.647 ± 0.054	0.330 ± 0.055
Uniform ($\epsilon = 32/255$)	0.251 ± 0.000	0.735 ± 0.052	0.425 ± 0.059
Uniform ($\epsilon = 128/255$)	0.502 ± 0.000	0.941 ± 0.057	0.623 ± 0.054

C.3 Variances decomposition and SNR measurements

To quantify the relative contributions of input v.s. internal variability, we randomly selected 50 images from the CIFAR-10 test set. For each image, we generated 50 uniform noise perturbations within a fixed $\ell_\infty = 8/255$ norm bound and passed each perturbed input through the diffusion model using 50 different random seeds. This resulted in a total of 125,000 purification images. We then estimated the variance components and SNR as defined. The results are summarized in Table S5 and S6.

Table S5: Variances and SNRs in diffusion purification / $\times 10^{-3}$.

Total Var.	Input Var.	Internal Var.	SNR
3.597 ± 0.877	0.020 ± 0.005	3.578 ± 0.873	5.926 ± 1.065

Table S6: ℓ_2 Distances to corresponding centroids in diffusion purification.

Initial	Fix Inputs	Fix Random	Vary Both
1.004 ± 0.001	0.241 ± 0.032	3.282 ± 0.453	3.288 ± 0.453

C.4 The effect of timesteps on clean accuracy and compression rates

We investigated the effect of timesteps on compression rate, robustness and clean accuracy. As timesteps increases, the clean accuracy drops monotonically, as there are more samples mis-purified into different classes. Intriguingly, for reverse-only diffusion models, we observed a S-shape trend on the compression rates, which can be divided into three regimes (Fig. S4b). In low timesteps (0-200), compression rates decreases as timesteps increases. In medium timesteps (200-700), there is a increase of compression rates, which constraints the robustness improvements. Lastly in the high timesteps (700-1000), the compression rate further reduces, but due to the low clean accuracy, the robustness improvement is also limited. However, we did not observe the same trend for DiffPure methods, as the compression rate is monotonically decreasing (Fig. S4a).

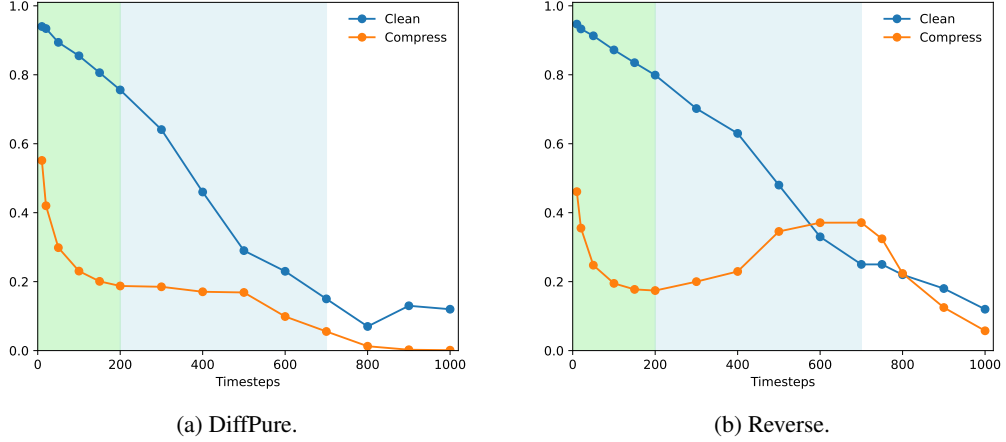


Figure S4: The effect of timesteps on clean accuracy and compression rates.

Table S7: List of existing assets.

Existing Assets	License
CIFAR-10 (Krizhevsky & Hinton, 2009)	Unknown
ImageNet (Deng et al., 2009)	Custom (research, non-commercial)
DDPM (Ho et al., 2020)	MIT
Guided diffusion (Dhariwal & Nichol, 2021)	MIT
Foolbox (Rauber et al., 2020)	MIT
AdverTorch (Ding et al., 2019)	GNU v3
RobustBench (Croce et al., 2020)	MIT
PyTorch-FID (Heusel et al., 2017; Seitzer, 2020)	Apache v2

D Computational resources and reproducibility

We conduct our PGD/BPDA experiments on Nvidia GeForce 3080Ti GPU. The PGD/BPDA experiments on CIFAR-10/ImageNet took around 24 hours for each repeat with a batchsize of 1 on our subsampled dataset. For PGD/BPDA-EOT experiments, we rent Nvidia H100 GPU (80GB), and the experiments took around 120 hours for batchsize of 1. The codebase will be open-sourced in the camera-ready version once published.

E Broader impact

This paper discusses how and how well do diffusion models actually improve robustness. Randomness can induce gradient masking and can not easily solved by the previous standard EOT method, which raises ethical concerns for the actual robustness improvements for previous adversarial purification works (Nie et al., 2022; Xiao et al., 2023; Lee & Kim, 2023; Li et al., 2025). The identified lawful relation between compression rates and robustness improvements may lead to the design of safer machine learning systems benefiting the society.

F Licenses for existing assets

The licenses for existing assets are listed in Table S7. URLs are documented in implementation details in Appendix B.